Contract # WC133R-1O-CN-0212

HF Radar Calibration with Automatic Identification System Ships of Opportunity

Phase II Final Report

Chad Whelan, Calvin Teague and Donald Barrick
Codar Ocean Sensors, Ltd.

Brian Emery and Libe Washburn
Marine Science Institute, University of California Santa Barbara

EXECUTIVE SUMMARY

Under Phase I of this SBIR program, CODAR Oceans Sensors and the University of California, Santa Barbara (UCSB) demonstrated the feasibility of using AIS vessel positions to identify vessel echoes in HF Radar Doppler cross spectra and the characteristics of those echoes to produce antenna pattern measurements (APMs). Under Phase II, the primary objective was the development of an operational prototype. To attain this objective, software for processing the AIS and HF radar data was integrated with 3rd party commercial AIS hardware to operate with SeaSonde® data collection computers, outputting antenna pattern data in real time. The prototype developed under Phase II is now close to commercial readiness and the first commercial version is on schedule to be offered within three months of the completion of this phase II program. The technical objectives described in the Phase II work plan were attained as follows: 1) software for automated real time APM determination was developed and deployed; 2) quantitative data quality indicators were developed and improved compared to Phase I methods; 3) azimuthal coverage was expanded compared with Phase I results; and 4) these methods were applied to systems operated at other commonly used HF radar frequencies bands. With this augmentation, SeaSonde operators will be able to calibrate antenna patterns in a less expensive and time-consuming manner, which will both save money and foster higher quality data outputs for Search and Rescue, Spill response activities as well as the many other uses identified by the NOAA Integrated Ocean Observing System (IOOS).

This material is based upon work supported by the Department of Commerce under contract number WC133R-1O-CN-0212. Any opinions, findings, conclusions or recommendations expressed in this publication are those of the author(s) and do not necessarily reflect the views of the Department of Commerce.

I. INTRODUCTION

Due to their ability to map surface currents from shore with high temporal and spatial resolution, HF radar has become a key component of coastal ocean observing systems. Of the approximately 300 HF radars operating in real time globally, about 130 are operated in the U.S. with funding provided by the National Oceanic and Atmospheric Administration (NOAA) Integrated Ocean Observing System (IOOS). Typical applications, including oceanographic research, search and rescue (SAR) operations, and hazardous material spill response, all benefit from accurate HF radar surface current measurements.

The antenna pattern describes the response of the receive antennas to an arriving signal as a function of bearing. Any HF Radar must perform an accurate determination of bearing in order to produce valuable surface current maps and so an accurate representation of the antenna pattern is essential. Several studies have demonstrated improved comparisons between HF radar and in situ ocean current measurements when using a measured pattern (APM) for bearing determination (Barrick and Lipa, 1999, Kohut and Glenn, 2003, Paduan et al. 2006). Best practices for the operation and maintenance of HF radars prescribe regular measurement of antenna patterns as a necessary component of the quality assurance and quality control (QA/QC) of HF radar data (Cook et al., 2012). Traditionally, this has involved moving a signal source, such as a transponder, around the receive antenna so that the signal can be used to calibrate the antenna response at all bearings from which sea echo is received. At many sites, this involves putting the transponder on a boat, which costs time and money and is dependent on local weather conditions. Therefore, an automated method for determining APMs would assist operators in the QA/QC of HF radar data. Additionally, precise, high-resolution antenna patterns are even more important for successful deployment of emerging bi-static and multi-static HF radar systems as well as applications like vessel detection.

The approach for measuring antenna patterns described here uses vessels of opportunity that transmit their positions using the Automated Identification System (AIS). Vessel echoes appear often in HF Radar Doppler spectra and software has been developed at CODAR to remove these echoes from surface current processing as well as detect vessels. These echoes, like any source signal, can provide antenna pattern information for the Radar at the bearing to the vessel, but without a method of knowing the bearing to the vessel, then the antenna pattern information in the echo is of little value. AIS, designed and used primarily for collision avoidance, broadcasts ship identification, position and velocity information every 2-10 s while underway. The broadcasts include ship identification (Maritime Mobile Service Identity (MMSI)), latitude, longitude, speed, and heading and can be received using low-cost equipment and software. The AIS system operates in the maritime VHF band, with an operational range on about 100 km, depending strongly on the height of the AIS transmitter on the vessel and the height of the receiver on shore. The AIS supplies critical position data for using vessel HF radar echoes to derive antenna patterns.

This report documents the NOAA SBIR Phase II development of a general method and prototype for the automatic measuring of antenna patterns for DF-type HF radars using ships of opportunity broadcasting with AIS. The Phase II technical objectives are:

1. Refine algorithms to calibrate antenna patterns automatically in real-time as a substitute for more costly, infrequent transponder-based calibrations;
2. Develop quantitative indicators of the quality of the ship-derived antenna patterns;
3. Expand the azimuthal coverage of ship-derived antenna pattern measurements and increase the amount of pattern data produced over time.
4. Apply the ship-based antenna pattern method to other commonly used frequency bands including those operating at frequencies around 5, 25 and 42 MHz.

The work plan for obtaining these technical objectives is stated:

1. Obtain additional development data sets of AIS and HF radar cross-spectra with a broad range of transmit frequencies and levels of ship traffic;
2. Implement existing ship detection algorithms to improve separation of ship backscatter from other cross-spectral components and to eliminate ship size as a criterion for measuring patterns;
3. Develop data quality metrics based on comparisons with transponder-measured patterns, and use these to produce robust averages of ship-derived patterns;
4. Develop operational code to ingest AIS data, merge these with HF radar cross-spectra, and apply algorithms to produce real-time antenna pattern measurements;
5. Develop operational code to quantify antenna pattern statistics and to detect change through time.

This report demonstrates how the technical objectives were attained during Phase II research. Section II describes data quality methods developed during Phase II, including how ship signal can be identified in HF radar data and some methods used to produce antenna pattern estimates from ship backscatter. Section III describes technical details of the prototype development, including hardware integration with operational software. Section IV shows the results of algorithm improvements, the metrics used to improve the methods, and the patterns produced by the prototype. In section V we discuss the implications and conclusions of these results.

II. Data Quality Metrics & Quality Control

Part of the algorithm development during Phase II included data quality metrics and AIS-based thresholds for improving the APM results. This work followed the work plan as stated:

> *Develop data quality metrics based on comparisons with transponder-measured patterns, and use these to produce robust averages of ship-derived patterns; Implement existing ship detection algorithms to improve separation of ship backscatter from other cross-spectral components and to eliminate ship size as a criterion for measuring patterns*;

The resulting metrics and thresholds are based on characteristics of the signal measurements and ship AIS data. These were developed by comparing with transponder measured patterns ($\mathbf{A}_{TRANS}$), enabling the production of APMs at HF radar sites with previously undetermined APMs. Prior to demonstrating the data quality metrics developed in Phase II, we restate the comparison metric, which forms an objective measure of the difference between transponder-measured and ship-based patterns. This can then be minimized when searching for metrics to quantify error, or alternatively data quality.

a. Comparison Metric

At each bearing, we quantify the difference between complex vectors $\mathbf{A}_{SHIP}$ and $\mathbf{A}_{TRANS}$ using the Euclidean distance (D) between the two at the same bearing. Before computing D, $\mathbf{A}_{SHIP}$ and $\mathbf{A}_{TRANS}$ are put into an equivalent form consisting of only real numbers. The vector $\mathbf{A}$ is rewritten in terms of the real and imaginary components:

$$\mathbf{A} = [\mathrm{Re}(a_1(\theta))\ \mathrm{Im}(a_1(\theta))\ \mathrm{Re}(a_2(\theta))\ \mathrm{Im}(a_2(\theta))]^T \quad (1)$$

The component a_3 is dropped from the expression, since it always has $\mathrm{Re}(a_3) = 1$, and $\mathrm{Im}(a_3) = 0$. Simplifying the notation, the subscripts R and I designate real and imaginary components:

$$\mathbf{A} = [a_{1R}\ a_{1I}\ \ a_{2R}\ a_{2I}]^T \quad (2)$$

Eq. (2) gives the four components of $\mathbf{A}(\theta)$ as a vector of real numbers. For two estimates of the antenna pattern at a given bearing (e.g. $\mathbf{A}_{SHIP}(\theta)$ and $\mathbf{A}_{TRANS}(\theta)$), the Euclidean distance D is defined,

$$D(\theta) = [\ (\mathbf{A}_{SHIP}(\theta) - \mathbf{A}_{TRANS}(\theta)^T\ (\mathbf{A}_{SHIP}(\theta) - \mathbf{A}_{TRANS}(\theta))\ ]^{1/2} \quad (3)$$

b. Signal-to-noise ratios

Investigations identified four signal-to-noise ratios (SNRs) for use as data quality metrics, to separate ship backscatter from other signal sources. Cross spectra recorded by HF radars contain various signal components, including first and second order backscatter from the ocean surface, broadband and narrowband noise from other HF radar transmitters, natural external sources including worldwide thunderstorms, as well as backscatter from ships. The SNRs are designed to identify ship backscatter signal that is free of signals from these other sources. When measuring antenna patterns with transponders, the signal is ideally characterized by a narrow peak in both frequency and range, with power levels well above the noise. Away from the peak, the signal level ideally falls rapidly to background noise levels in adjacent bins and adjacent range cells. When used with thresholds, the SNRs identify ship backscatter data that fits this general description. Each of the four SNRs is produced according to the equation,

$$SNR = S_{SIGNAL} - \langle S_{NOISE} \rangle \qquad (4)$$

where S_{SIGNAL} is the power observed (dBm) in the monopole auto spectra, in the range cell and Doppler bin assumed to contain ship backscatter. $\langle S_{NOISE} \rangle$ is the average of bins assumed to contain only noise, as explained below.

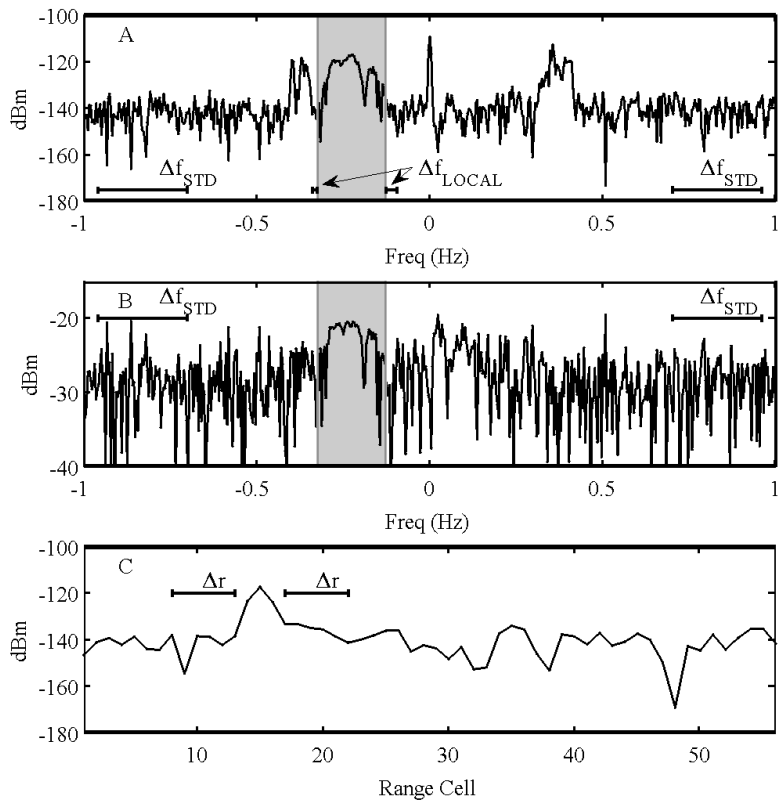

Fig. 1. a) HF radar cross spectra as a function of frequency (from Fig. 2c) along with the ship radial velocity from AIS (gray shaded area), for range cell 15. Horizontal bars near the bottom of the figure show range of frequency (Δf) over which average noise levels are computed for SNR_{STD} and SNR_{LOCAL}. b) Remaining cross spectra signal after removing hourly mean, along range of frequency (Δf) over which average noise levels are computed for SNR_{TIME}. c) Cross spectra plotted as a function of range cell index, for the frequency bin centered at -0.227 Hz. Horizontal bars show the range cells (Δr) used to compute the average noise level for SNR_{RANGE}, spanning range cells 8-13 and 17-22.

The first SNR, denoted SNR_{STD}, is computed from Eq. (4) with $\langle S_{NOISE} \rangle$ computed as the average power over two frequency ranges, Δf_{STD} = 0.701 to 0.960 Hz, and -0.701 to -0.960 Hz, (Fig. 1a). SeaSonde software typically uses noise levels in the region defined by Δf_{STD} to compute SNR of the first order Bragg scatter peaks. Following the SeaSonde method, an initial $\langle S_{NOISE} \rangle$ is obtained, then spectral points more than three standard deviations from the mean are removed and $\langle S_{NOISE} \rangle$ is recomputed on the remaining points.

The second SNR, $SNR_{LOCAL,}$ is computed using Eq. (4) after computing $<S_{NOISE}>$as the mean spectral power spanning a range of Doppler frequency bins (Δf_{LOCAL}) adjacent to the ship peak. Here $<S_{NOISE}>$ is computed from 20 Doppler bins found on either side of the spectral region identified by AIS (Fig. 1a). Bragg signals are excluded from this calculation, such that the resulting mean may depend on fewer than the 40 Doppler bins.

The third SNR, SNR_{RANGE}, is computed using Eq. (4) with $<S_{NOISE}>$ determined from multiple range cells. Unlike SNR_{STD} and SNR_{LOCAL}, which are computed in single range cells, SNR_{RANGE} is computed using $<S_{NOISE}>$ based on spectra power found in the same Doppler bin (f_{SHIP}), but in several range cells spanning two intervals (Δr). The Δr intervals each span five range cells, beginning two range cells away from S_{SIGNAL}. For example, if the ship S_{SIGNAL} is located in range cell 15 and Doppler bin f_{SHIP}, $<S_{NOISE}>$ is computed from signals found at f_{SHIP} in the Δr intervals extending between range cells 8-13 and 17-22, as shown in Fig. 1c. The Δr intervals begin two range cells away from $S_{SIGNAL,}$ because some ship backscatter signal may be present in adjacent range cells due to pulse stretching in the receiver (Lipa and Barrick 1983). Both SNR_{LOCAL} and SNR_{RANGE} are measures that have been used in SeaSonde vessel detection algorithms and in recording direct signal parameters received from other SeaSondes with synchronized waveforms.

The fourth SNR, SNR_{TIME}, uses the time domain properties of both S_{SIGNAL} and $<S_{NOISE}>$ to separate short term signal sources, such as ships, from persistent signal sources, such as currents and waves. Prior to the Eq. (4) calculation, the time-centered, hourly averaged cross spectrum is subtracted from the individual cross spectra containing S_{SIGNAL}. As shown in Fig. 1b, this removes much of the first and second order Bragg signal, along with any other signals persisting on hourly or longer time scales. SNR_{TIME} is then computed with Eq. (4) using S_{SIGNAL} from the residual, and $<S_{NOISE}>$ over Doppler regions defined by Δf_{STD} as in SNR_{STD}. Calculation of SNR_{TIME} is similar to real time HF radar processing methods, which apply an Infinite Impulse Response (IIR) filter to identify and remove ship backscatter (Barrick et al. 1994).

The above methods produce four SNRs for each signal observation that may contain ship backscatter. Low SNR from any of the four methods suggests the presence of contaminating interference or other non-ship signal. When applying thresholds to the SNRs, the lowest value of SNR of the four prevents the $\mathbf{A}_{SHIP}$ point from passing a given SNR threshold. Thus the minimum of the four methods is found,

$$SNR_{MIN} = \min(SNR_{STD}, SNR_{LOCAL}, SNR_{RANGE}, SNR_{TIME}) \quad (5)$$

such that each $\mathbf{A}_{SHIP}$ observation is associated with one SNR value for use in thresholding.

c. AIS based thresholds

Three additional metrics are computed from the AIS data for use in thresholding. The first is the standard deviation of the ship radial velocity observed during the 256-s cross spectra interval (σ_{SHIP}). $\mathbf{A}_{SHIP}$ observations obtained from ships when $\sigma_{SHIP} > 150$ cm s^{-1} were excluded from the analysis. The second metric is the distance between ships and oil platforms (Δd_p). $\mathbf{A}_{SHIP}$ exhibits large errors when ships are close to these structures, and so ships with $\Delta d_p < 1500$ m were excluded. The third metric Δd_s is defined as the minimum separation in range and Doppler bins between ships. This metric identifies ships that are in nearly the same range cell and traveling at nearly the same radial velocity relative to a site. Ships separated by $\Delta d_s < \pm 1$ range cell and $< \pm 20$ Doppler bins were excluded. Note that ship length, which is typically available in the AIS data and was used in the Phase I analysis, is no longer used as a threshold, attaining the stated technical objective.

d. Assigning bearing

The final step in the determination of $\mathbf{A}_{SHIP}$ is to associate observations of the antenna pattern in $\mathbf{A}(\theta_j)$ to the ship bearing θ_j. From the AIS latitude and longitude, reported at approximately 10 s intervals, time-centered radial velocities are computed along with the corresponding bearing to the HF radar, producing a time series of ship radial velocity and bearing. These observations form a table during the time of the 256 s FFT. Recall that the FFT separates signal into bins as a function of Doppler frequency, or equivalently radial velocity. Thus each signal bin and corresponding Doppler radial velocity is associated with the ship radial velocity and a bearing to the ship within the FFT time through a table lookup. This method enables more precise association of ship position than would an average of the ship position data over 256 s.

III. Product Development

a. Software Architecture

Under phase II, four components of the envisioned software package were developed at CODAR: 1. AIS collection, decoding and logging (*AISLogger*), 2. AIS data webserver for serving the local AIS data (*AISWebServer*), 3. Software to match AIS data to the SeaSonde site and spectral data (*AISTracker*) and software to take the relative vessel positions and match with the echoes found in the cross spectra to produce an antenna pattern (*AISLooper*). These components were developed with the idea of building a commercial software package. The modular nature of the software was designed so that each may operate independently allowing for the ability to separate the AIS data collection from the HF Radar site and pattern processing and allow reprocessing from multiple stages of data collection. The four software components are described below.

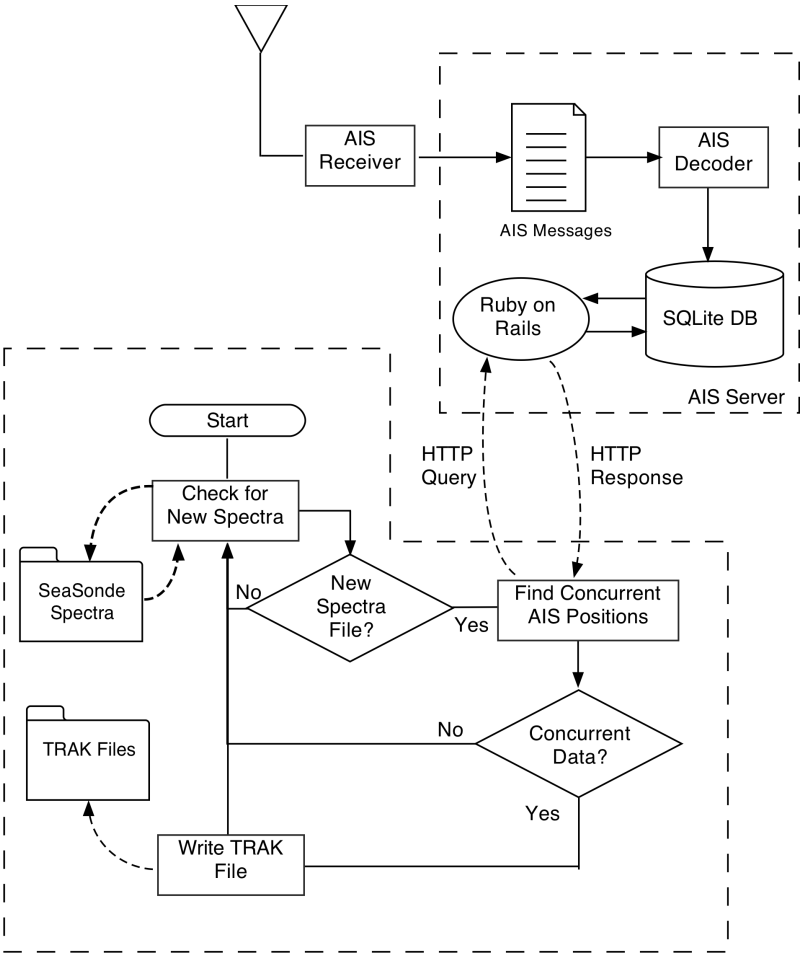

Fig. 2: Flow diagram of the AIS data collection, decoding and formatting. TRAK files are then used to search cross spectra files for suitable vessel echoes.

b. AIS Decoding, Logging and the Database

A system daemon starts a ruby script, which opens a 38,400 kbps serial stream over the USB port connected to the AIS receiver. Each AIS message received by the hardware is transmitted as a coded ASCII line. The same ruby script then calls the *ais.py* decoding script for each AIS message that arrives. Sometimes several messages per second will be seen, and at other times several minutes may go by without any messages.

The AIS protocol is extensive and is documented in considerable detail as part of the open-source GPSd project. The source code for that project includes a Python script, *ais.py*, which decodes most of the AIS messages. There are 27 basic message types, and some of the basic messages have 10 or 20 subtypes, so the protocol is large, but only a very few of the AIS messages are relevant to the automatic SeaSonde antenna calibration procedure. In particular, types 1, 2, 3 and 18 (ship position reports), type 4 (base station reports), and type 5 (ship static information) are decoded and logged. A few others (types 15 and 20) are recognized and silently discarded, and other types are noted as “not processed”.

If the message is one of the types mentioned above, the raw message fields are converted to metric engineering units, tagged with the computer time when the message was received and then saved into an SQLite database. The SQLite engine is included as part of the standard Macintosh operating system, so it is convenient to use for this application. SQLite also allows for flexible searching of AIS data by time, position or vessel ID (MMSI). The raw message, along with the time tag, is also logged to a text file in case offline reprocessing of the raw messages is desired. The text files all have a date as part of their name, and new files are started at each computer reboot (typically once per day or once per week). The text output to the log file looks as follows:

*2013-09-13T23:59:32Z !AIVDM,1,1,,B,176tdG002LG;kdDEIjmo0UU600S=,0*07*
*2013-09-13T23:59:51Z !AIVDM,1,1,,A,152dQf001no9SEhEPwvCojs80@E=,0*25*
*2013-09-13T23:59:51Z !AIVDM,1,1,,B,15RdL8001;o=NHTE`q5TfSg80<1V,0*5D*
*2013-09-13T23:59:51Z !AIVDM,1,1,,B,18;CI>002uo=>Q@E1:e=Sbm<0<1S,0*01*
*2013-09-13T23:59:52Z !AIVDM,1,1,,B,133whj0viFo<KLPEJLV7WV=80HFR,0*46*
*2013-09-13T23:59:52Z !AIVDM,1,1,,A,Dh3Ovk0m9N>4g@fGLfpNfp0,2*7D*
*2013-09-13T23:59:52Z !AIVDM,1,1,,B,Dh3Ovk0s=N>4g<fGLfpNfp0,2*18*
*2013-09-13T23:59:52Z !AIVDM,1,1,,A,4h3Ovk1unFos`o>jOJEdjIg02L2q,0*5D*
*2013-09-13T23:59:52Z !AIVDM,1,1,,B,4h3Ovk1unFos`o>jOJEdjIg02L2q,0*5E*

c. AIS Web Server

The database is served via the web through a simple Ruby on Rails process, which also runs as a system daemon. Thus, the web server is available whether or not any user is logged in. The browser interface of the server is intentionally kept extremely simple, just presenting tables of data, because the primary purpose of the web server is to listen for computer-generated data requests. Nevertheless, simple manually-generated requests from a browser are useful to check the operation of the logger and web server. There are two reasons we have enabled web access to the database. The first is that it is actually simpler than using command line tools and system calls. Second, it allows the AIS hardware and database to reside in a separate location than the SeaSonde computer. This allows the AIS receiver to be placed in a more advantageous location (height, unobstructed view) for receiving the VHF AIS signals than the SeaSonde computer site might allow. Additionally, a single AIS receiver can provide data to multiple SeaSondes.

d. AIS Track Generation

The AIS Track Generation process runs as a launch agent at periodic intervals, every 10 minutes, by default. It runs completely independently of the AIS logging process above. A ruby script searches for new CSQ files (raw cross spectra) and, for each one, calls the *AISTracker* program, passing it a series of command-line arguments. One of those arguments is the URL of the AIS web server, as specified by the user. By default, that URL is on the local machine, but it can be changed to point to an external address if the AIS web server is running on a different machine. If the vessel position table lookup returns positions with a time stamp in the time interval covered by the CSQ file, *AISTracker* writes a file with vessel positions and velocities relative to the SeaSonde providing spectral data and in standard CODAR TRAK file format with additional columns related AIS derived information. In total, 16 columns of data are in the track file:

TIME: *Time from start of track file*
BEAR: *Bearing to Vessel (from SeaSonde Rx Antenna)*
DIST: *Distance to Vessel (from SeaSonde Rx Antenna)*
RDIR: *Vessel's direction of travel along radial bearing from Rx Antenna*
RVEL: *Vessel's component of velocity along radial bearing from Rx Antenna*
LATD: *Latitude of vessel*
LOND: *Longitude of vessel*
TDIR: *Vessel's true course*
TVEL: *Vessel's true velocity*
MMSI: *Vessel AIS ID*
TYRS: *Year of AIS message*
TMON: *Month of AIS message*
TDAY: *Day of AIS message*
THRS: *Hour of AIS message*
TMIN: *Minute of AIS message*
TSEC: *Second of AIS message*

e. Antenna Pattern Generation

Also run as an independent launch agent, the program *AISLooper* takes the CSQ files that match the times of the TRAK files. *AISLooper* uses the vessel range and radial velocity (Doppler) information found in the TRAK file to find the ship echo in the cross spectra. It then records the spectral parameters of the vessel echo at the Doppler bin associated with the reported radial velocity component of the vessel speed along with the bearing to the vessel, which is also found in the TRAK file. Additional metadata about the vessel echo is also recorded for further filtering and quality control. In total, 33 columns of data & metadata are contained in the LOOP file:

TRGB: *Bearing to Vessel (from SeaSonde Rx Antenna)*
A13M: *Signal amplitude ratio (antenna 1 ÷ antenna 3)*
A13P: *Phase difference (antenna 1 – antenna 3)*
A23M: *Signal amplitude ratio of (antenna 2 ÷ antenna 3)*
A23P: *Phase difference (antenna 1 – antenna 3)*
AR3D: *Absolute vessel echo peak magnitude (dBm)*
AR3P: *Absolute vessel echo peak phase (deg)*
TRGD: *Vessel's direction of travel along radial bearing from Rx Antenna*
TRGV: *Vessel's component of velocity along radial bearing from Rx Antenna*
PKRC: *Peak range cell # (integer)*
PKDC: *Peak Doppler bin # (relative to DC - 0 Hz Doppler)*
A1SN: *Signal-to-noise of peak on channel 1*
A2SN: *Signal-to-noise of peak on channel 2*
A3SN: *Signal-to-noise of peak on channel 3*
A1NF: *Noise floor at edge of Doppler window on channel 1*
A2NF: *Noise floor at edge of Doppler window on channel 2*
A3NF: *Noise floor at edge of Doppler window on channel 3*
A1CF: *Noise floor around vessel echo peak on channel 1*
A2CF: *Noise floor around vessel echo peak on channel 2*
A3CF: *Noise floor around vessel echo peak on channel 3*
RCEN: *Range cell # centroid calculation (can be fractional)*
DCEN: *Doppler bin # centroid calculation (can be fractional)*
PKR1: *Echo peak edge starting range cell #*

PKR2: *Echo peak edge ending range cell #*
PKD1: *Echo peak edge starting Doppler bin #*
PKD2: *Echo peak edge ending Doppler bin #*
A1AB: *Signal-to-noise ratio on channel 1 using IIR background removal*
A2AB: *Signal-to-noise ratio on channel 2 using IIR background removal*
A3AB: *Signal-to-noise ratio on channel 3 using IIR background removal*
TGID: *Vessel AIS ID*
FLAG: *Flag data that meets certain criteria*
DATE: *Date string*
TIME: *Time string*

The result is a LOOP file that contains raw vessel position and spectral echo parameters. Each LOOP file contains antenna pattern data for one day, by default, but could be set to weekly or monthly files. Currently, analysis of this LOOP file requires a trained technician in order to produce an antenna pattern for use in the standard SeaSonde current processing algorithms.

f. Quality Control Integration

A MATLAB® script has been developed that trained CODAR technicians use to sort, filter and plot the antenna pattern data. The script will open as many LOOP files as are available and can analyze antenna pattern data over an hour, a day, a month or however much time there is data available. The technician has the option to filter the data based on the following parameters:

Minimum/Maximum Signal-to-Noise Threshold
Minimum/Maximum Signal-to-Noise (w/ IIR average removed) Threshold
Maximum Range Peak Width
Minimum/Maximum Doppler Peak Width
Minimum/Maximum Range
Minimum/Maximum Vessel Speed
Minimum # of Echoes in Bearing Window
Time/Data range
Individual Vessels

The technician can adjust the thresholds of the above parameters to maximize confidence in the resulting pattern and/or reduce thresholds to allow for greater coverage. In the event that the above parameters still leave what appears to be erroneous solutions, the technician can hand edit the solutions to achieve the desired pattern. Raw pattern solutions are reduced to values on bearing a increment, usually 1° - 5°, by one of three methods: median, mean or SNR weighted mean of all the solutions falling within a range around each bearing.

g. AIS Hardware Integration

One of the primary tasks of phase II was to develop a real-time antenna pattern collection capability. In order to do this, we need to integrate a real-time AIS data stream into the SeaSonde data processing computer. After some investigation into AIS services and hardware options, the choice was made to incorporate the Comar AIS-2-USB AIS Receiver, a USB-powered dual channel input AIS receiver whose core chipset is

designed by FTDI (http://www.ftdichip.com/) who provide drivers for many USB-to-serial devices on a wide variety of platforms including Mac OS X, the operating system used by SeaSonde data collection computers. During phase II, however, this model was made obsolete by the Comar AIS-3R (see Figure 3), which allows dual USB and serial outputs. This may be advantageous to those customers who would like an AIS stream independent of the SeaSonde computer. Both models are low-power (powered by USB bus only) and provide a local real-time stream of AIS messages via USB directly to the computer. With a small physical footprint (longest dimension is 5 inches), the Comar AIS-3R can be easily added to almost any enclosure containing the SeaSonde electronics. Additional advantages are that hardware installation will not require a trained CODAR technician, any VHf antenna covering the AIS bands (161.975 MHz and 162.025 MHz) can be used and the hardware can be separated from SeaSonde site if more a desirable location for VHf AIS transmissions is available nearby (e.g. a tall building within a few km of the SeaSonde).

Fig. 3. Image of Comar AIS-3R AIS receiver

IV. RESULTS

a. Comparison with Phase I methods

Technical objectives of the Phase II work plan included, 1) remove ship length criteria, 2) improve azimuthal coverage, and 3) increase pattern data produced in time. All three of these objectives were met through the improvements in thresholding and screening criteria described above. The improvements are demonstrated in Fig. 4, which compares results at the end of Phase 1 (green) vs. the end of Phase 2 (blue). For each of the four HF radar sites, the number of data points per 5° bin remaining after thresholding is plotted vs. bearing, based on the same initial AIS and HF radar data sets. Removing ship length criteria, varying how SNR is computed, and implementing the time domain SNR calculation resulted in significant increases in the amount of usable data. Fig. 4 also shows the increase in the total number of data points, which ranged between about a factor of two (SCI, 12685 to 29576), to a factor of about five (MGS, 516 to 2790). The improved efficiency of the method is demonstrated by the fact that the increases in N where observed for relatively small increases in the number of unique ships providing the data. For example, the factor of five increase in N at MGS came from only a factor of 1.3 more ships. The increases in usable data also translated into improved azimuthal coverage demonstrated by Fig. X. Observations span a greater range of bearings overall at all sites, with increases ranging from about 20° to 60°.

b. Data Quality Metrics

Using D as a quantitative indicator of error between $\mathbf{A}_{SHIP}$ and $\mathbf{A}_{TRANS}$, or alternatively as a data quality indicator, we investigated metrics that minimize D. The result of these investigations indicated that the best metric is given by SNR_{MIN}. Values and scatter of error (as illustrated by D) decrease rapidly with increasing SNR_{MIN} at all four sites (Fig. 5). For SNR greater than 10 dB, the broad scatter in D narrows, such that $SNR_{MIN} > \sim 15$ dB is associated with low D. SCI is an exception with some points with $SNR_{MIN} > 10$ and $D \sim 1.25$. Values of D averaged over bins of width $\Delta SNR = 1$ dB are also shown (open circles), along with the number N of points per bin (right-hand y-axis) showing that each site has more than 1000 observations with $SNR_{MIN} > 10$.

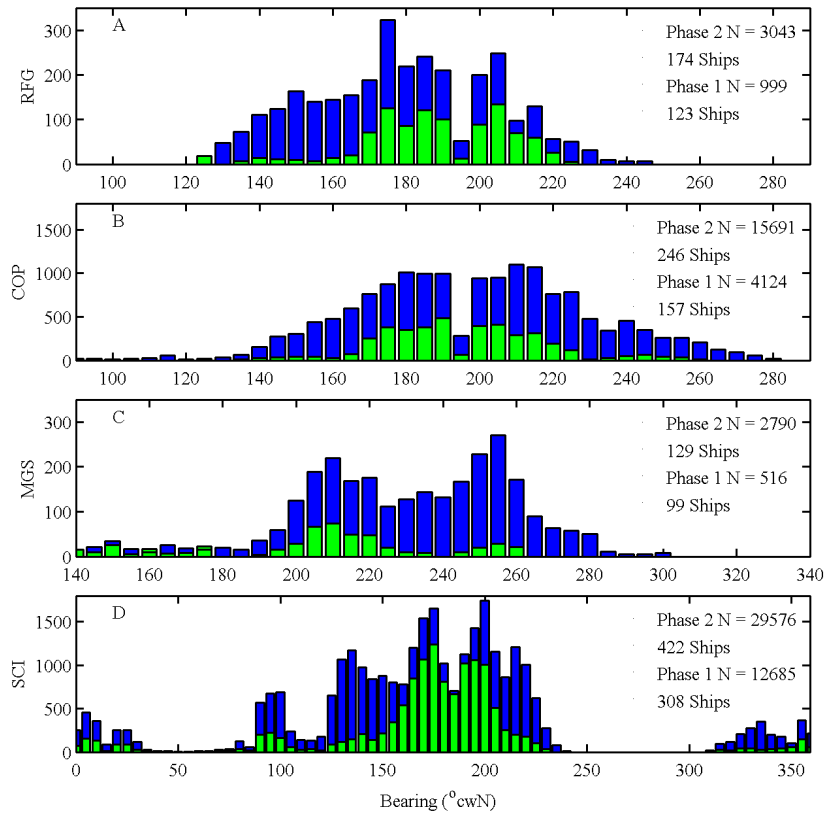

Fig. 4. Comparison of results from Phase I with Phase II. The number of data points per 5° bin is plotted (Phase I, green, Phase II in blue) for each of the four UCSB HF radar sites; a) RFG, b) COP, c) MGS and d) SCI. The total number of data points and ships are also shown.

A desirable outcome of this research is to assess feasibility of the method as an independent source of antenna pattern measurements. In estimating $\mathbf{A}_{SHIP}$, significant agreement between $\mathbf{A}_{SHIP}$ and $\mathbf{A}_{TRANS}$ was found (e.g. Fig. 5) when the following empirical thresholds were used:

- $SNR_{MIN} > 11$ dB
- $\sigma_{SHIP} < 150$ cm s^{-1}
- $\Delta d_p > 1500$ m

- $\Delta d_s >$ ±1 range cell and > ±20 Doppler bins

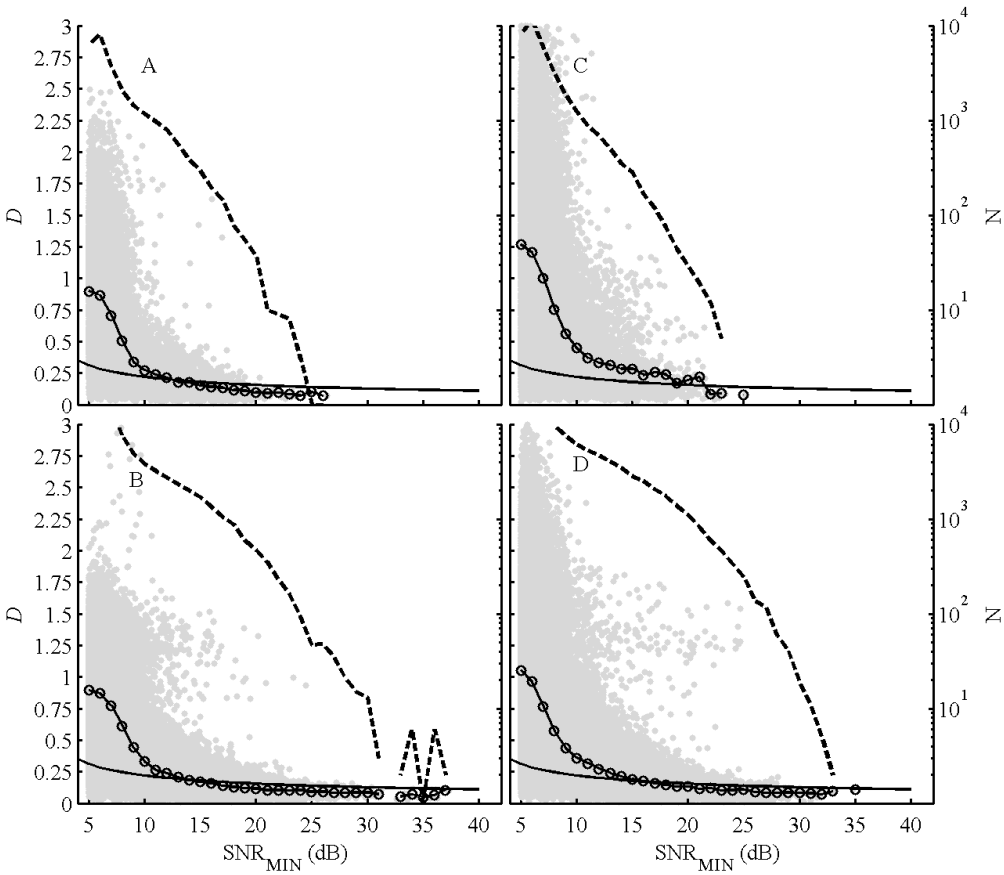

Fig. 5: D vs. SNR_{MIN} (gray dots, left axis), with their bin average (open circles, left axis), and N data points per bin on a log scale (dashed line, right axis). Theoretical error given by Barrick (2003) is also shown (solid line, left axis) after converting degrees to D. For a) RFG, b) COP, c) MGS and d) SCI.

Figure 5 guided the choice of the SNR_{MIN} threshold, which produces low overall error as measured by *D*. Limiting the standard deviation of radial velocity (σ_{SHIP}) identifies ships with smoothly varying radial velocity and slowly changing position during the 256-s integration times of the cross spectra. Both Δd_p and Δd_s thresholds removed multi-source signals, which produced errors in $\mathbf{A}_{SHIP}$. Each threshold is applied to metrics computed directly from the AIS and HF radar data, demonstrating the feasibility of the method as and independent source of APMs.

These results corroborate a previous theoretical and experimental analysis of ship tracking with HF radars that found a power law relationship between SNR and the bearing error (Barrick, 2003). Linearly relating *D* to the bearing error in degrees, the Barrick (2003) result can be used to show a theoretical *D* as a function of SNR. The theoretical *D* vs. SNR plotted on Figs 5a-d shows reasonable agreement with observed

values of D for $SNR_{MIN} > 10$. The Barrick (2003) analysis suggests rejecting data with SNR below 7-10 dB, in agreement with the Fig. 5 results.

In addition to errors resulting from low overall SNR, some scatter in $\mathbf{A}_{SHIP}$ may result from errors in the AIS and the GPS positions they report. Methods used to assign bearings to $\mathbf{A}_{SHIP}$ described previously depend on associating the radial velocity of the received signal with the ship position when the signal was backscattered. GPS errors, radial velocity errors due to ship motions (pitch and roll) and aliasing of these motions contribute to errors in the determined bearing. To put an upper bound on the errors from these sources, the standard deviation of the bearings traversed by the ship during the FFT window is computed (Table 1). Errors in AIS bearings to the ships are likely much less than the approximately 2-3° standard deviations. Fig. 5 indicates that errors in $\mathbf{A}_{SHIP}$ are on the order of $D \sim 0.2$, which our analysis suggests is equivalent to about 12°. Thus errors in bearing resulting from GPS and other position errors are likely a small fraction of the error in the estimated $\mathbf{A}_{SHIP}$ components.

Table 1. Statistics of bearings traversed by ships during FFT windowing time, as observed by each HF radar site.

Site	Mean (o)	Stdev (o)	Max (o)	Min (o)	Median (o)	N
COP	3.32	2.32	37.3	0.005	2.95	4687
RFG	3.95	3.38	20.2	0.030	2.95	1178
MGS	3.19	1.87	20.0	0.015	2.92	1218
SCI	2.28	1.63	20.9	0.004	1.99	8702

d. Frequency of pattern generation

This analysis can address two additional questions regarding the opportunistic generation of patterns from ships. First, how frequently can $\mathbf{A}_{SHIP}$ be generated? Figure 6 shows the ratio $N_{SHIP}(t)/N_{TRANS}$ where $N_{SHIP}(t)$ is the number of estimates of $\mathbf{A}_{SHIP}(\theta)$ at unique bearings θ at 1° resolution accumulated during time t; N_{TRANS} is the total number of bearings in $\mathbf{A}_{TRANS}$ at 1° resolution. The times required to generate $\mathbf{A}_{SHIP}(\theta)$ for various SNR_{MIN} are shown by the different lines. For example, Figure 6a shows that $\mathbf{A}_{SHIP}$ at RFG covers about 75% of the 1° bearings of $\mathbf{A}_{TRANS}$ with $SNR_{MIN} > 10$ after 60 days. COP (Fig. 6b) covers about 95% of bearings during the same time period. $\mathbf{A}_{SHIP}$ covering 75% of $\mathbf{A}_{TRANS}$ with $SNR_{MIN}>10$ can be generated in approximately 53 days at RFG, 9 days at COP, 12 days at MGS, and 2 days SCI. Of course these times depend on the level of ship traffic.

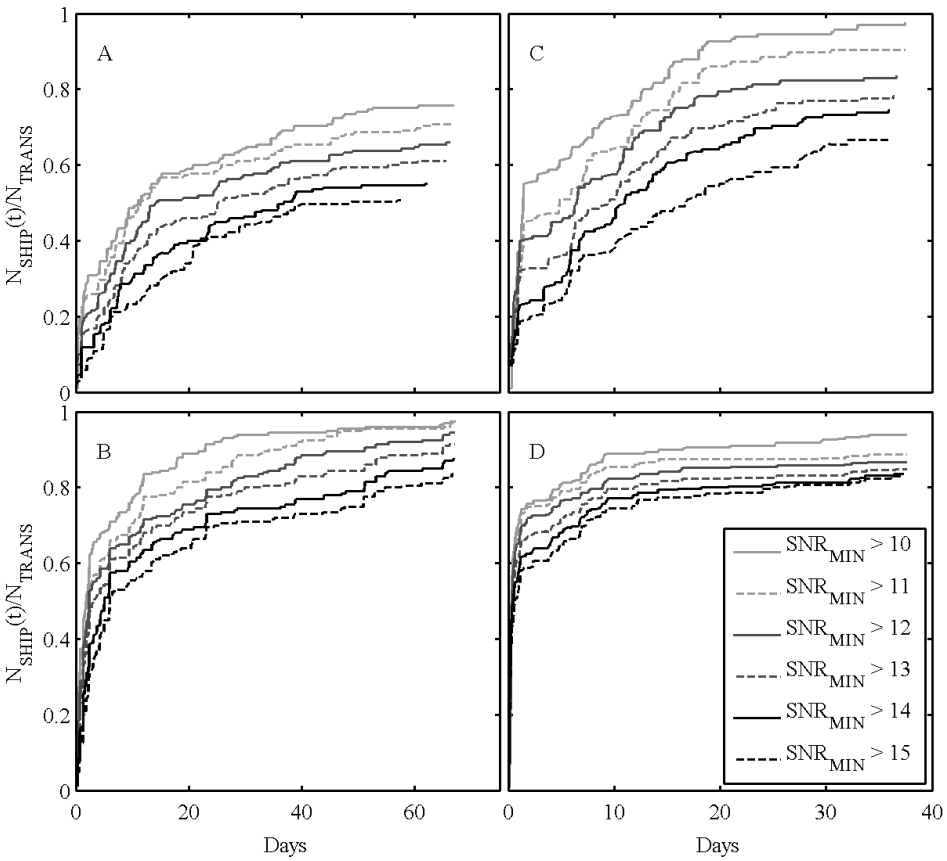

Fig. 6: Curves showing the ratio $N_{SHIP}(t)/N_{TRANS}$ vs. time in days. The five curves for each subplot are for different SNR_{MIN} thresholds (legend, Fig. 6 d). Gaps resulting from HF radar or AIS outages where truncated to one day. For a) RFG, b) COP, c) MGS and d) SCI.

Second, how many ships are needed to generate a pattern? This question can be answered by substituting the number of ships n for time t to obtain the ratio $N_{SHIP}(n)/N_{TRANS}$.. Figure 7 shows that $\mathbf{A}_{SHIP}$ covering 75% of $\mathbf{A}_{TRANS}$ with SNR_{MIN}>10 can be generated from155 ships at RFG, 50 ships at COP, 48 ships at MGS, and 47 ships at SCI.

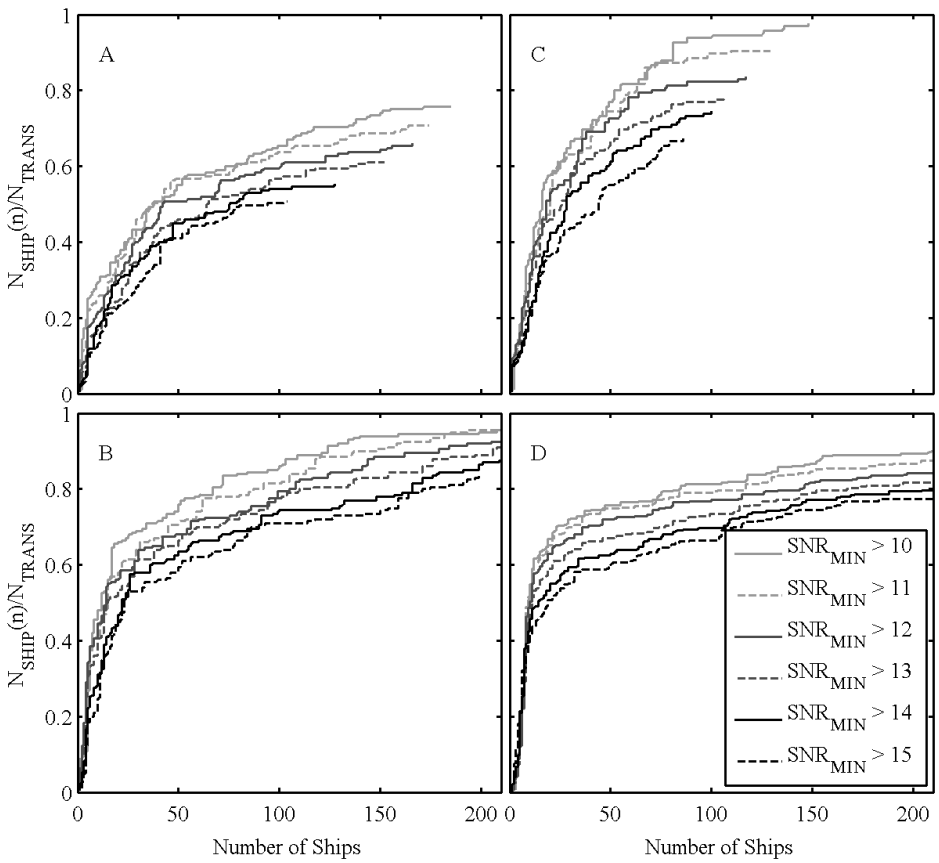

Fig. 7: Curves showing the ratio $N_{SHIP}(n)/N_{TRANS}$ vs. the number of unique ships. The five curves for each subplot are for different SNR_{MIN} thresholds (legend, Fig. 7 d). For a) RFG, b) COP, c) MGS and d) SCI.

e. Product beta deployment results

A beta version of the product has now been installed on eight operational field sites as follows:

FORT (13 MHz): Fort Funston, San Francisco, CA
BML1 (13 MHz): Bodega Marine Lab, Bodega, CA
BMLR (5 MHz): Bodega Marine Lab, Bodega, CA
YHL1 (5 MHz): Yaquina Head, OR
NORD (13 MHz): Nordøy Island, Norway
EPSM (13 MHz): Cabo Espichel, Portugal
VIEW (25 MHz): Ocean View Park, Chesapeake Bay, VA
SUNS (25 MHz): Sunset Pier, Chesapeake Bay, VA

These sites were chosen for a variety of transmit frequency, vessel density and location (domestic U.S. west coast, east coast and international). The results below are drawn from 10 days of measurements from the beta product installed at the Ocean View Beach Park (VIEW), a 25 MHz site located on the southern shoreline of the Chesapeake Bay in Norfolk, VA with a viewing azimuth spanning -55° T CW to 110° T. This is a high vessel density area and 742,151 AIS messages were received over the ten days.

Figure 8 shows the 4,151 filtered vessel echo derived pattern solutions from left to right and top to bottom [Re$(a_1(\theta))$ Im$(a_1(\theta))$ Re$(a_2(\theta))$ Im$(a_2(\theta))$] in red. The number of AIS messages per day fluctuated between 300 and 700. Filtering was done using the following criteria for the characteristics of the vessel echo peak:

```
Minimum SNRloc = 15 dB
Maximum SNRloc = 40 dB
Maximum Range Width = 3 cells
Minimum Doppler Width = 3 Doppler bins
Maximum Doppler Width = 10 Doppler bins
Maximum Range = 40 km
```

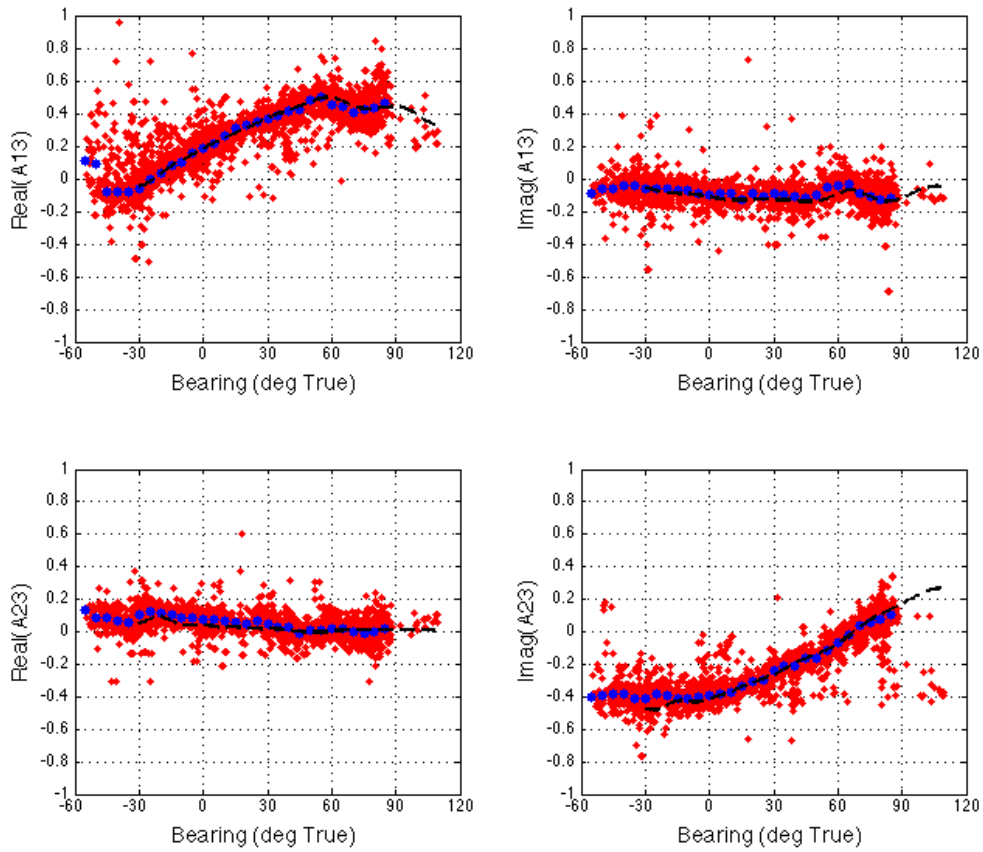

Figure 8: VIEW antenna pattern. Real and imaginary components for Loop 1 (a & b) and Loop 2 (c & d). Blue circles represent 5°median filter of vessel solutions (red). 15 dB SNR threshold was used. Black (- -) represents the prior transponder-measured antenna pattern.

In order to produce a useable pattern, the filtered points are reduced to one solution per bearing increment by median filtering. In this case, a 5° bearing increment is used. The antenna pattern as measured by a transponder is shown as black dashed line. Figures 9 and 10 below show the resulting pattern in amplitude and phase, respectively, as dots versus the transponder measurement as dashed line. From the plots it appears that the transponder measurement does not extend as far on the West side of the pattern and vessel echoes do not extend as far as the transponder pattern to the East. There are also some notable differences between the two, indicating that the pattern has changed since the last transponder measurement or that one of the methods is faulty.

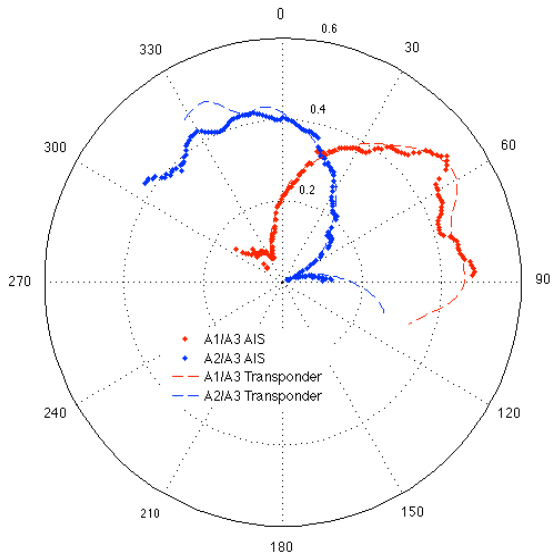

Figure 9: Polar plot of relative loop antenna amplitude response patterns with 15 dB SNR Threshold. Loop 1 (red) and Loop 2 (blue) are shown. Patterns from transponder are plotted as -- and from vessel echoes plotted as '.'

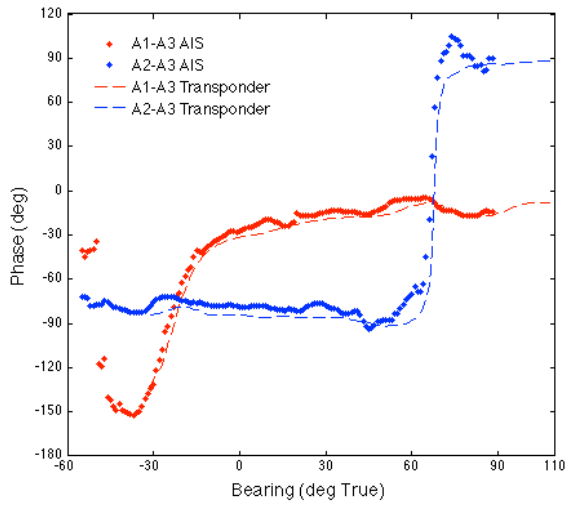

Figure 10: Polar plot of relative loop antenna phase response patterns with 15 dB SNR Threshold. Loop 1 (red) and Loop 2 (blue) are shown. Patterns from transponder are plotted as -- and from vessel echoes plotted as '.'

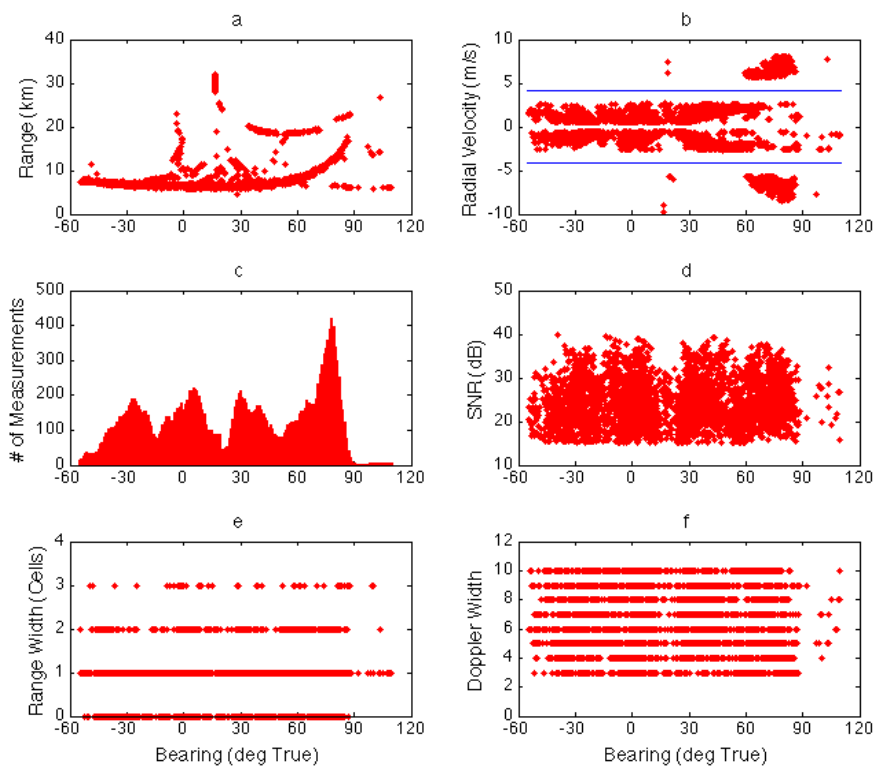

Figure 11: Metadata vs. bearing for VIEW antenna pattern shown in Figures 18-20: a) vessel range, b) radial velocity, c) number of solutions, d) SNR (dB), e) peak width (range), and f) peak width (Doppler).

Figure 11(a) through (f) show some metadata for the filtered 4,151 points. This metadata is produced in real time and can provide some feedback of ship behavior and signal characteristics. The metadata will be critical for SeaSonde technicians to evaluate the performance of the software as well as optimize default values so the software can do the filtering and producing patterns in real time little or no post processing.

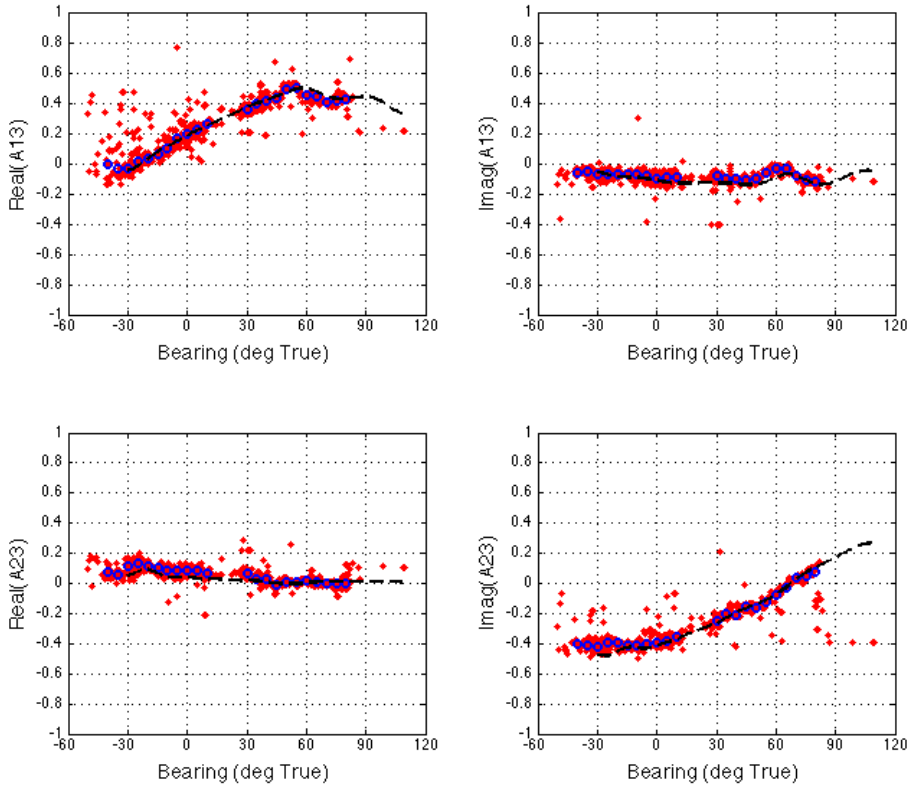

Figure 12: See Figure 8 for description. 25 dB SNR Threshold used

If we increase the SNR threshold to 25 dB, we reduce the number of measurements from 4151 to 810, as shown in figure 12 above. There is much less spread in the data and tighter correlation with the measured pattern. The cost is the azimuthal coverage reduces about 10° to 20° on either end and a 15° gap appears between 10° T and 30° T.

If SNR threshold is decreased to 6 dB, as shown below in Figures 13 - 15, the number of filtered measurements increases to 11,098 and there is quite a bit more spread in the measurements. The accuracy, as measured by comparing the antenna pattern derived from median filtering the vessel with the transponder-derived pattern, remains the same or is slightly improved. The real benefit is that the azimuthal coverage is improved so that vessel echoes are detected over the entire necessary range to resolve the pattern from -55°T to 110°T.

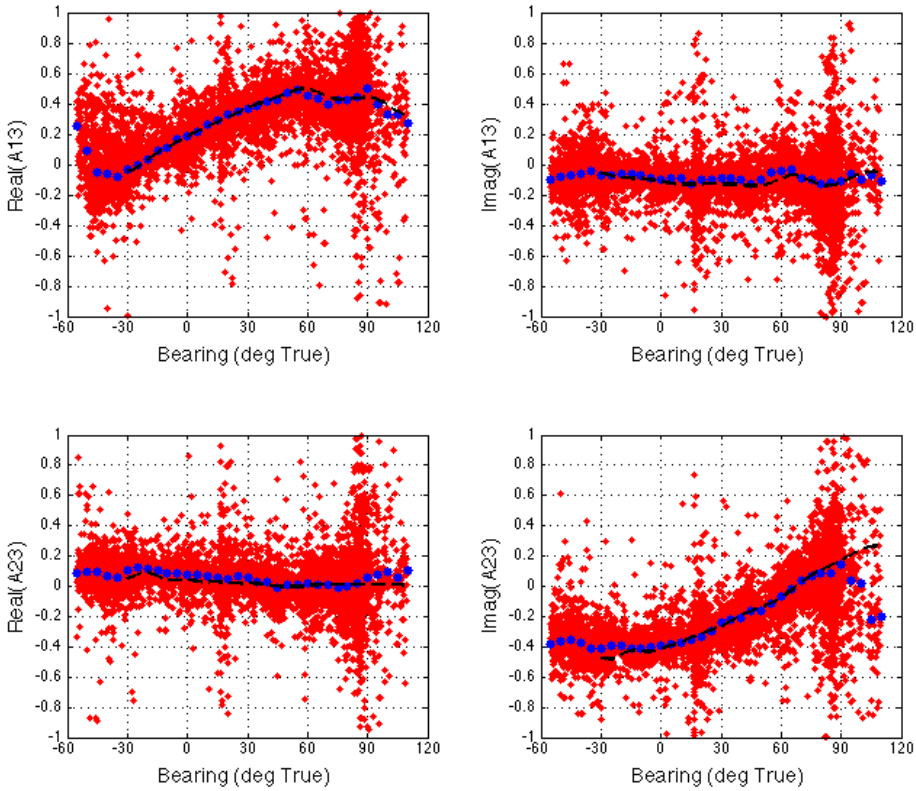

Figure 13:See Figure 8 for description. 6 dB SNR Threshold

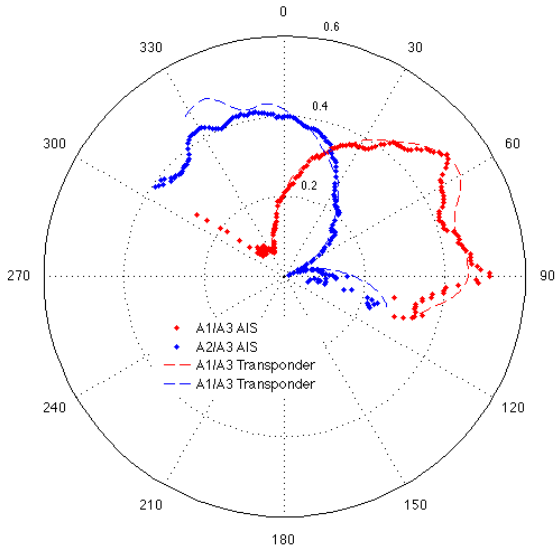

Figure 14: Polar plot of relative loop antenna amplitude response patterns with 6 dB SNR Threshold. Loop 1 (red) and Loop 2 (blue) are shown. Patterns from transponder are plotted as -- and from vessel echoes plotted as '.'

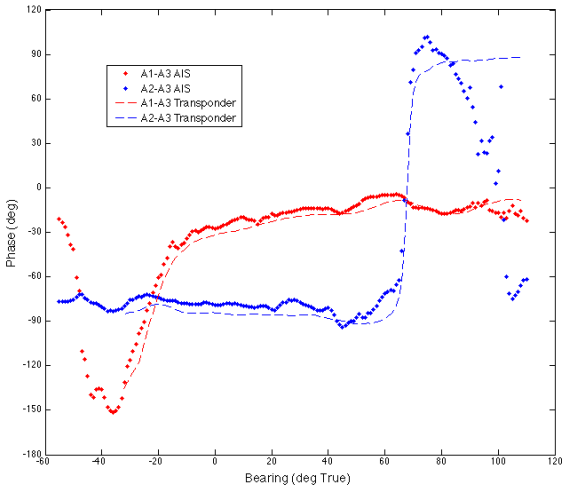

Figure 15: Plot of relative loop antenna phase response patterns with 6 dB SNR Threshold. Loop 1 (red) and Loop 2 (blue) are shown. Patterns from transponder are plotted as -- and from vessel echoes plotted as '.'

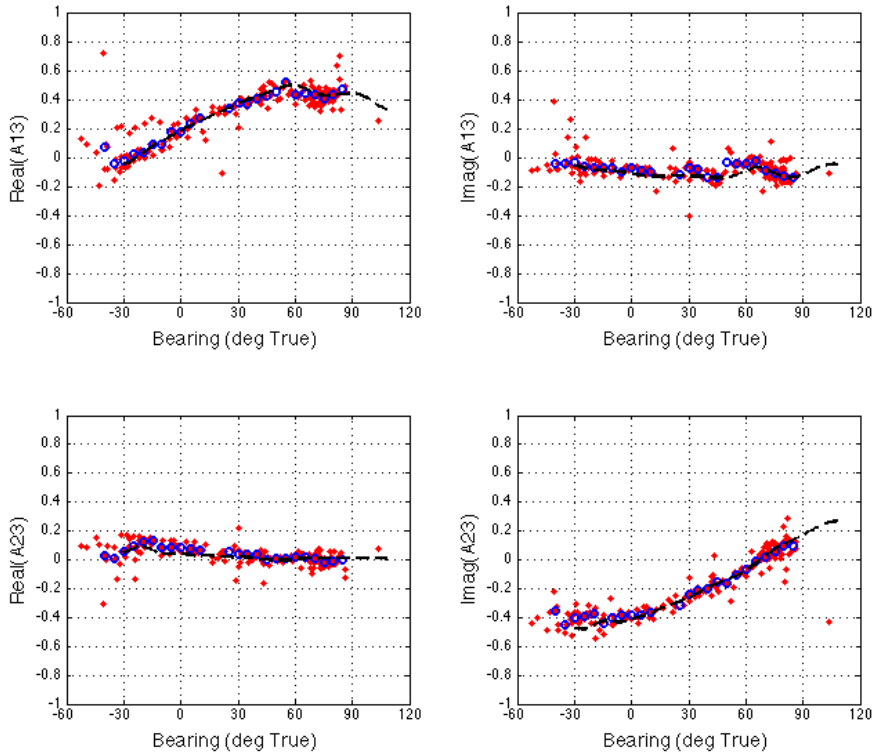

Figure 16: See Figure 8 for description. 15 dB SNR Threshold (200 point random sample of 4151)

For a trained technician to analyze the pattern, it is a good practice to know how few points should be relied upon to trust an antenna pattern or, as discussed in IV d above, how quickly can a pattern be updated. Additional filtering of the data applied by a technician will reduce the amount available for pattern analysis. In order to gauge how few points could be used to resolve the pattern, the 15 dB SNR filtered data was randomly sub-sampled to see at what number of measurements the pattern was no longer "useable". Figure 16 shows the results after sub-sampling 200 measurements. The azimuthal coverage is reduced on the edges by ~10°, but the accuracy does not appear to have suffered and there is only on small gap of 5°. Figure 17 shows the results of sub-sampling only 100 points. While 100 points may be suitable for detecting gross changes in loop antenna amplitudes or phases, it appears that setting a limit of ~200 measurements is necessary to produce a "usable" pattern. This, of course, assumes that the azimuths are somewhat evenly distributed in azimuth as they are at VIEW site. This is a little higher but same order of magnitude as the results shown in section IV d above.

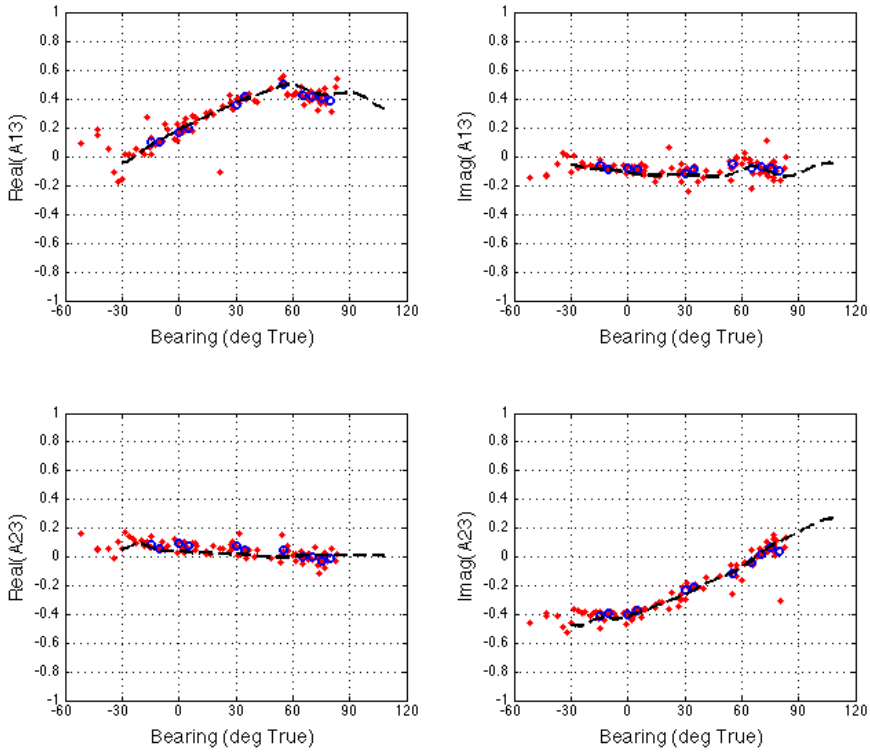

Figure 17: See Figure 8 for description. 15 dB SNR Threshold (100 point random sample of 4151)

Other sites will have different vessel paths and densities. Figures 18 – 20 show antenna pattern data for Bodega Marine Lab Long Range Seasonde (BMLR), located in Bodega, CA - North of San Francisco Bay. This site operates in the 5 MHz band. The antenna pattern shown in Figures 18-20 was derived from vessel echoes over a 145-day span from 1 May 2013 through September 23, 2013 and comprised 1,273,308 AIS messages.

As shown in Figure 21 a) & c), the distribution of vessels is quite different from VIEW. Most of the vessels at BMLR appear in the Southwest quadrant between 170° T and 270° T where most of the shipping lanes from San Francisco Bay are located. However, this site needs to resolve surface currents beyond 270° up to ~320° T. Out of the 1,273,308 AIS messages, only 8,508 messages were left after thresholding with 15 dB SNR and in the sector from 270° to 320° T, each 5° bearing increment had between 10 and 50 solutions over the entire period. For certain sites, there will be sectors with low vessel density. These sectors will require more time and perhaps be subject to noisier measurements of the antenna pattern. This will be part of the analysis performed after collecting data over the first few weeks or months after installation.

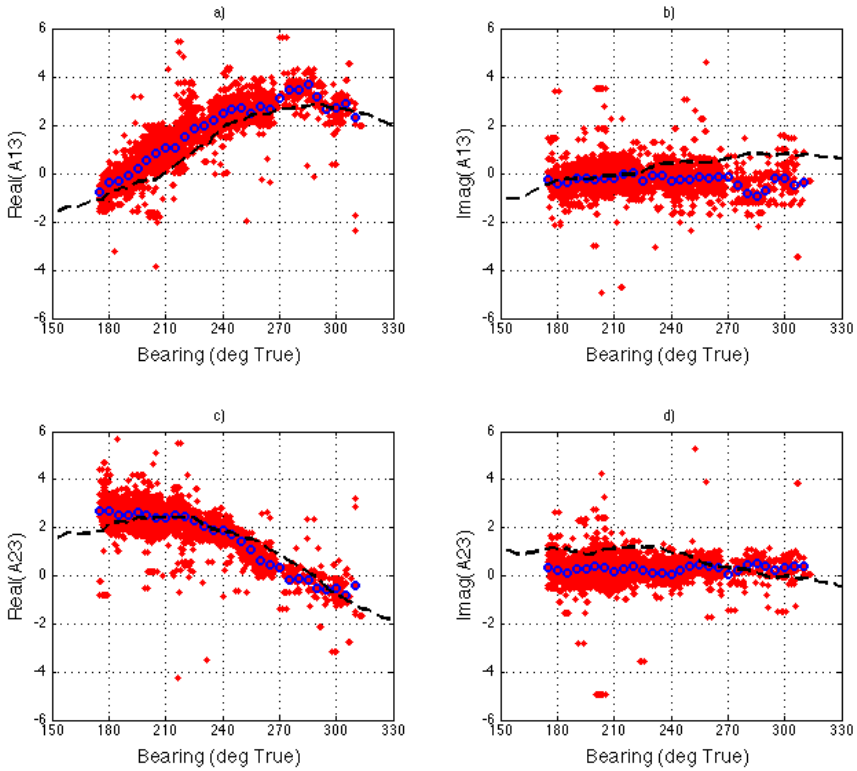

Figure 18: BMLR antenna pattern. Real and imaginary components for Loop 1 (a & b) and Loop 2 (c & d). Blue circles represent 5°median filter of vessel solutions (red). 15 dB SNR threshold was used. Black (- -) represents the prior transponder-measured antenna pattern.

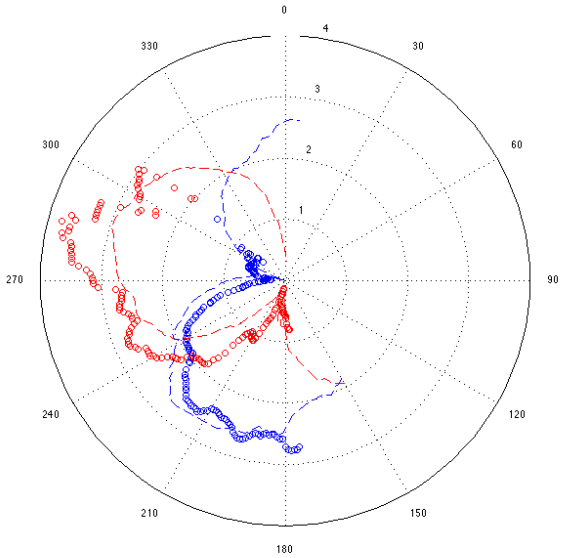

Figure 19: Polar plot of relative loop antenna amplitude response patterns for BMLR with 15 dB SNR Threshold. Loop 1 (red) and Loop 2 (blue) are shown. Patterns from transponder are plotted as -- and from vessel echoes plotted as '.'

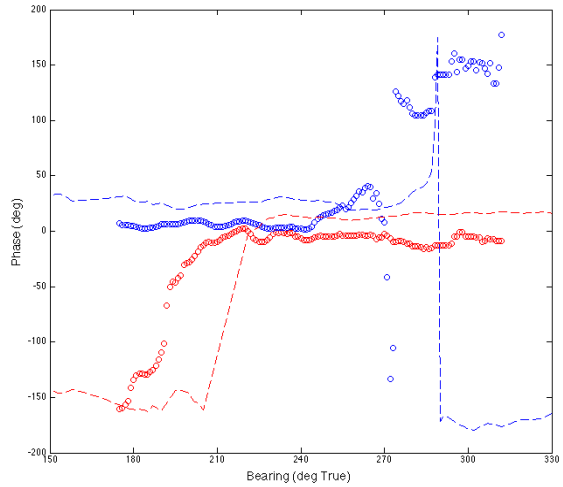

Figure 20: Plot of relative loop antenna phase response patterns for BMLR with 15 dB SNR Threshold. Loop 1 (red) and Loop 2 (blue) are shown. Patterns from transponder are plotted as - - and from vessel echoes plotted as '.'

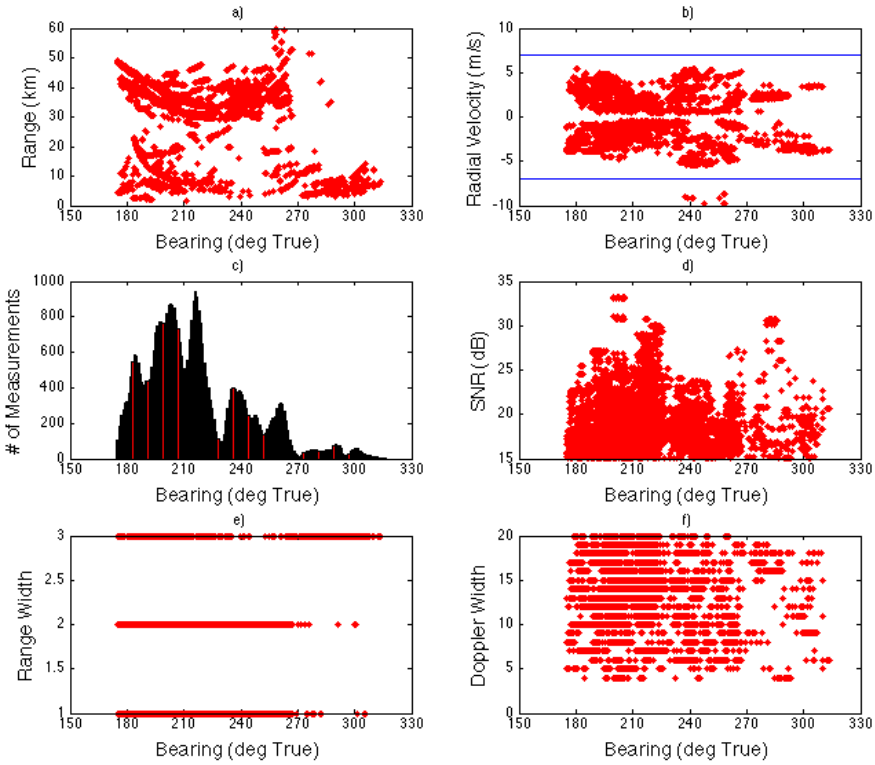

Figure 21: Metadata vs. bearing for BMLR antenna pattern shown in Figures 18-20: a) vessel range, b) radial velocity, c) number of solutions, d) SNR (dB), e) peak width (range), and f) peak width (Doppler).

V. CONCLUSIONS

This report details the technical objectives and work plan proposed in the NOAA SBIR Phase II, and how these objectives where attained through the combined efforts of investigators at CODAR Ocean Sensors and subcontractor UCSB. As proposed, real time software for automated APM determination was developed and deployed on 8 systems, both domestically and abroad, data quality metrics and algorithms for antenna pattern analysis were developed. Through an iterative process, quantitative data quality indicators were developed and improved. As demonstrated, the improvements increased azimuthal coverage compared with Phase I methods.

The primary objective of Phase II was the development of real-time operational software. To attain this objective, software for processing the AIS and HF radar data was integrated with 3rd party commercial AIS hardware to operate with SeaSonde data collection computers, outputting antenna pattern data in real time. The software developed under Phase II is now close to commercial readiness and the first commercial version is on schedule to be offered within three months of the completion of this phase II program. Because SBIR funds have provided for all the startup development funds, the sale price can be kept low, encouraging adoption.

With this augmentation, SeaSonde operators will be able to calibrate antenna patterns in a less expensive and time-consuming manner, which will both save money and foster

higher quality data outputs for Search and Rescue, Spill response activities as well as the many other uses identified by U.S. Integrated Ocean Observing System (US IOOS).

ACKNOWLEDGMENTS

We thank Megan McKenna and John Hildebrand, Scripps Institution of Oceanography, for the use of their AIS data. Boat operations by David Salazar, Cristoph Pierre and Eduardo Romero contributed to $\mathbf{A}_{\mathrm{TRANS}}$ measurements at the UCSB HF radar sites. Discussions with, and the work of Cyril Johnson improved $\mathbf{A}_{\mathrm{TRANS}}$ measurements and many aspects of this analysis.

Additionally, for use of their systems to test software, we would like to thank the Center for Innovative Technology, Old Dominion University, Oregon State University, Qualitas Remos, Instituto Hydrografico, Bodega Marine Lab & met.no for use of their systems to test the AIS software and hardware package as well as their time in providing feedback and installing AIS hardware at their sites.

Finally, we would like to thank the NOAA Small Business Innovative Research (SBIR) Office for providing the resources to make this project a reality and Dr. Jack Harlan of US IOOS for acting as technical advisor to this project.

REFERENCES

[1] Paduan, J. D., K. C. Kim, M. S. Cook, and F. P Chavez, 2006. Calibration and Validation of Direction-Finding High-Frequency Radar Ocean Surface Current Observations, IEEE J. of Oceanic Engineering, vol. 31, no. 4, DOI 10.1109/JOE.2006.886195

[2] Kohut, J. T. and S. M. Glenn, 2003. Calibration of HF radar surface current measurements using measured antenna beam patterns. J. Atmos. Ocean. Tech., 1303-1316.

[3] SCCOOS Best Practices Document (based on Radio-wave Operators Working Group meetings (ROWG)):http://cordc.ucsd.edu/projects/mapping/documents/SCCOOS-BestPractices.pdf

[4] HFR Network system calibrations (idealized or measured): http://www.sccoos.org/data/hfrnet/xml/stationStatus.php

[5] Fernandez, D. M., J. F. Vesecky, and C. C. Teague, 2003, Calibration of HF radar systems with ships of opportunity, Proc. Intl. Geosci. Remote Sens. Symp. (IGARSS), vol. 7, pp 4271-3.

[6] Fernandez, D. M., J. F. Vesecky, and C. C. Teague, (2006) Phase corrections of small-loop HF radar system receive arrays with ships of opportunity, IEEE J. of Oceanic Engineering, vol. 31, no. 4, DOI 10.1109/JOE.2006.886238

[7] D. E. Barrick, and B. J. Lipa (1999), Radar angle determination with MUSIC direction finding, U. S. Patent 5,990,834.

[8] Lipa, B.J. and D.E. Barrick (1983), Least-squares methods for the extraction of surface currents from CODAR crossed-loop data: Application at ARSLOE, IEEE J. Oceanic Engr., vol. OE-8, pp. 226-253.

[8] Barrick, D. E. and B. J. Lipa (1997), Evolution of bearing determination in HF current mapping radars, Oceanography, vol. 10, no. 2, pp. 72-75.

[9] Barrick, D.E., Lipa, B.J. (1999), Using antenna patterns to improve the quality of SeaSonde HF radar surface current maps, Proceedings of the IEEE Sixth Working Conference on Current Measurement, pp. 5-8, DOI 10.1109/CCM.1999.755204.

[10] de Paolo, T.; Cook, T.; Terrill, E.; , "Properties of HF RADAR Compact Antenna Arrays and Their Effect on the MUSIC Algorithm," OCEANS 2007 , vol., no., pp.1-10, Sept. 29 2007-Oct. 4 2007, doi: 10.1109/OCEANS.2007.4449265

[11] Schmidt, R. O., 1986: Multiple emitter location and signal parameter estimation. IEEE Trans. Antennas Propag., 34, 276–280.

[12] Barrick D., B. Lipa, P. M. Lilleboe, and J. Issacson, 1994: Gated FMCW DF Radar and Signal Processing for Range/Doppler/Angle Determination, U. S. Patent 5,361,072.

[13] Barrick D., Codar Ocean Sensors, cited 2003: Bearing Accuracy against Hard Targets with SeaSonde DF Antennas [Available online at www.codar.com/images/about/AngleAccuracy.pdf]